Science of the Total Environment 649 (2019) 75–89

Contents lists available at ScienceDirect

Science of the Total Environment

journal homepage: www.elsevier.com/locate/scitotenv

Spatial and temporal variability in extreme temperature and precipitation events in Inner Mongolia (China) during 1960–2017

Siqin Tong [a,b,c,1], Xiangqian Li [a,1], Jiquan Zhang [a,b,*], Yuhai Bao [c], Yongbin Bao [a], Li Na [a], Alu Si [a]

[a] School of Environment, Northeast Normal University, Changchun 130024, China
[b] Key Laboratory for Vegetation Ecology, Ministry of Education, Changchun 130024, China
[c] College of Geography, Inner Mongolia Normal University, Hohhot 010022, China

HIGHLIGHTS

- Warm extreme indices significantly increased, while cold extreme indices decreased.
- Nighttime warming was higher than daytime warming in Inner Mongolia.
- Extreme temperature and precipitation events had long-range correlation based on DFA.
- ENSO, AO, and IOD had positive (or negative) impacts on warm (or cold) extremes.

GRAPHICAL ABSTRACT

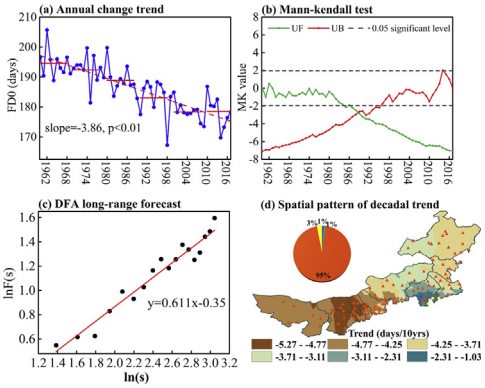

Linear regression trend (a), Mann-Kendall abrupt change detection (b), DFA long-range forecasting (c), and spatial pattern of decadal trend (d) of frost days (FD) during 1960-2017.

ARTICLE INFO

Article history:
Received 1 May 2018
Received in revised form 14 August 2018
Accepted 20 August 2018
Available online 21 August 2018

Editor: Jay Gan

Keywords:
Extreme climate events
Spatial and temporal variation
Detrended fluctuation analysis
Atmospheric circulation
Influence
Inner Mongolia

ABSTRACT

Due to global warming, extreme climate events have become an important issue, and different geographical regions have different sensitivities to climate change. Therefore, temporal and spatial variations in extreme temperature and precipitation events in Inner Mongolia were analyzed based on the daily maximum temperature, minimum temperature, and precipitation data during the period of 1960–2017. The results showed that warm extreme indices, such as SU25, TX90p, TN90p, and WSDI, significantly increased, whereas the cold extreme indices, such as FD0, TX10p, TN10p, and CSDI, significantly decreased; all indices have obvious abrupt changes based on the Mann-Kendall test; nighttime warming was higher than daytime warming. Extreme precipitation indices slightly decreased overall. All of the extreme temperature and precipitation indices had long-range correlations based on detrended fluctuation analysis ($a > 0.5$), thereby indicating that the extreme climate indices will maintain their current trend directions in the future. ENSO, AO, and IOD had a strong positive influence on warm extremes and a strong negative influence on cold extremes in Inner Mongolia. NCEP/NCAR and ERA-20CM reanalysis showed that strengthening anticyclone circulation, increasing geopotential height, decreasing daytime cloudiness and increasing nighttime cloudiness contributed to changes in climate extremes in Inner Mongolia.

© 2018 Elsevier B.V. All rights reserved.

* Corresponding author at: School of Environment, Natural Disaster Research Institute, Northeast Normal University, Changchun 130117, China.
E-mail address: zhangjq022@nenu.edu.cn (J. Zhang).
[1] Siqin Tong and Xiangqian Li equally contributed to this work.

https://doi.org/10.1016/j.scitotenv.2018.08.262
0048-9697/© 2018 Elsevier B.V. All rights reserved.

1. Introduction

The IPCC SREX (2012) reported that an extreme event is generally defined as the occurrence of a weather or climate variable at a value above (or below) a threshold value that is near the upper (or lower) ends ("tails") of the range of observed values of the variable. In recent years, the global climate has continuously warmed, and extreme climate events have occurred frequently (Leonard et al., 2013; Hao et al., 2013). This has resulted in a clear upward trend in the occurrence of meteorological disasters and has increased socioeconomic losses (Botzen and van den Bergh, 2009). According to recent statistics, the economic losses caused by global climate change and associated extreme weather events have increased by 10 times over the past 40 years (Ding et al., 2002). Asia is one of the continents that most frequently suffer from natural disasters, and natural disasters accounted for 43% of all extreme climate events in the world from 1990 to 2000, and the trend was becoming more serious after entering the 21st century with the global warming (Hou et al., 2008). Observations have shown that regional climate change has resulted in changes in various natural and biological systems, such as glacial retreat, permafrost melting, and the extension of the growing season in mid-high latitude areas (Shea et al., 2015; Rangecroft et al., 2016; Douville, 2006). In recent years, a series of meteorological disasters around the world (such as Hurricane Andrew in Florida in 1992, a catastrophic flood in China in 1998, and large-scale snow disasters in 2008) have caused a large number of casualties and substantial economic losses. This shows that studying the changing controls on and formation mechanisms of extreme climate events is not only necessary for scientific development but is also an urgent requirement of society (Barrett et al., 2015).

At present, research on extreme climate events mainly includes the study of extreme values, intensity, frequency, and changing trends of various indices and also includes conducting analyses and discussing the various factors involved in extreme climate events, among other topics (Gao et al., 2015; Planton et al., 2008; BrÖ et al., 2004; Brown et al., 2010). Researchers have studied extreme temperature and precipitation and have found that extreme temperature changes are generally associated with global warming, while extreme precipitation changes are less spatially correlated with global warming, making their trends difficult to understand (Alexander et al., 2006; Anders and Jones, 2005; Aguilar et al., 2005; Hidalgo-Muñoz et al., 2011; Omondi et al., 2013; Coumou et al., 2013; Coumou and Rahmstorf, 2012).

The frequency and intensity of extreme climate events in China have changed since 1951. Zhai and Pan (2003) indicated that the frost period in the eastern part of northern China is lengthening, and the number of extreme precipitation events in the northwest is increasing. Ma et al. (2003) studied extreme temperatures in northern China and concluded that the occurrence frequency of the highest temperatures in most parts of the northern region showed a significant increasing trend after the 1990s; these researchers also noted that the decrease in the frequency of extreme low temperatures and the increase in the low temperatures themselves are closely related to regional warming. Additionally, researchers have studied extreme climate changes in Shandong, Xinjiang, Chongqing, eastern China, southern China, and the Yangtze River Basin (Jiang et al., 2011; Zhang et al., 2012; Su et al., 2017; Chen and Sun, 2015). These changes in extreme climate events are closely related to regional climate warming and atmospheric circulation (Diffenbaugh et al., 2017; Abiodun et al., 2013; Swain et al., 2016). Therefore, many large-scale atmospheric circulation indices, such as the El Niño Southern Oscillation (ENSO), Pacific Decadal Oscillation (PDO), Arctic Oscillation (AO), North Atlantic Oscillation (NAO) and Southern Oscillation (SO), were applied to examine these relationships (Pascual et al., 2013; Muhire et al., 2015; Zhou and Wu, 2010; Chan and Zhou, 2005; Suo et al., 2008; Wan et al., 2010; Gong et al., 2009). However, there is little research on the effects of multiple atmospheric circulation indices, such as ENSO, NAO, AO, the Indian Ocean Dipole (IOD), and PDO, on the temporal and spatial changes in extreme temperature and precipitation events in Inner Mongolia.

Inner Mongolia contains one of the largest grasslands in China and is an important ecological barrier in the north of China. It is also an important agricultural and animal husbandry production base in China (Sun and Wang, 2008). Thus, it is a sensitive area in terms of global warming (Wang et al., 2008). Vegetation coverage can reflect the overall condition of the ecological environment in Inner Mongolia; therefore, the change in vegetation and its relationship with climatic factors has been a topic of interest in the scientific community (Wang et al., 2010). The decline in water levels, grassland degradation, and land desertification are closely related to climate change. At present, many studies exist on temperature and precipitation in Inner Mongolia (Bao et al., 2010; Chen et al., 2009; Bao et al., 2011), but studies that analyze extreme climate events are rare. Therefore, it is necessary to conduct a comprehensive study on the characteristics and evolution of extreme climate events in Inner Mongolia by analyzing the extreme temperature and precipitation indices, influencing factors, and future predictions, which have great significance for predicting catastrophic climate events and preventing and reducing disasters in Inner Mongolia.

2. Data and methods

2.1. Study area

The Inner Mongolia autonomous region was selected as the study area. It is located in the northern part of the People's Republic of China and lies between 37°24′N and 53°23′N and 97°12′E and 126°04′E (Fig. 1a). It has a total area of approximately 1.18 million km^2, which occupies 12.3% of China's total area and makes it the third largest province in China. It is located in the interior of the Eurasian continent and is under the influence of the East Asian monsoon because it falls within the zone of transition between humid and semi-humid monsoon climate and arid and semiarid climate (Sun et al., 2010). Due to the gradient in rainfall and temperature, its vegetation types, from the northeast to the southwest, are forest, grassland, and desert (Shi et al., 2011). The annual mean air temperature progressively increases from approximately −4.5 °C in the northeast to 9.8 °C in the southwest (Fig. 1b), but the annual precipitation decreases from the northeast to the southwest (Fig. 1b). In addition, the elevation increases from the northeast to the southwest, ranging from 86 to 3526 m. Altitude also has an important influence on the distribution of temperature and precipitation; therefore, we use cokriging, a method that takes elevation into consideration, to interpolate the meteorological data and obtain the spatial distribution of extreme temperature and precipitation indices (Daly et al., 2003; Goovaerts, 2000).

2.2. Data sources and quality controls

The data used in this study were acquired from the Resource and Environment Data Cloud Platform (www.resdc.cn/), which included the daily maximum temperature, minimum temperature, and precipitation data during the period of 1960–2017.

Data quality control is necessary before the analysis of temperature and precipitation variation because erroneous outliers can impact trends (Gao et al., 2015). Data quality control was performed using RClimDex software (http://cccma.seos.uvic.ca/ETCCDI/software.shtml), which was developed and maintained by Zhang and Yang (Li et al., 2012) at the Climate Research Branch of the Meteorological Service of Canada. It was used to check for inaccurate temperature and precipitation data, such as precipitation values below 0 and minimum temperatures that exceed maximum temperatures. Additional quality control involved identification of potential outliers; in particular, identifying whether the recorded data were consistent with the actual meteorological conditions in the region. Three times the standard deviation was defined as the threshold for quality control of the data. This threshold can detect almost all erroneous

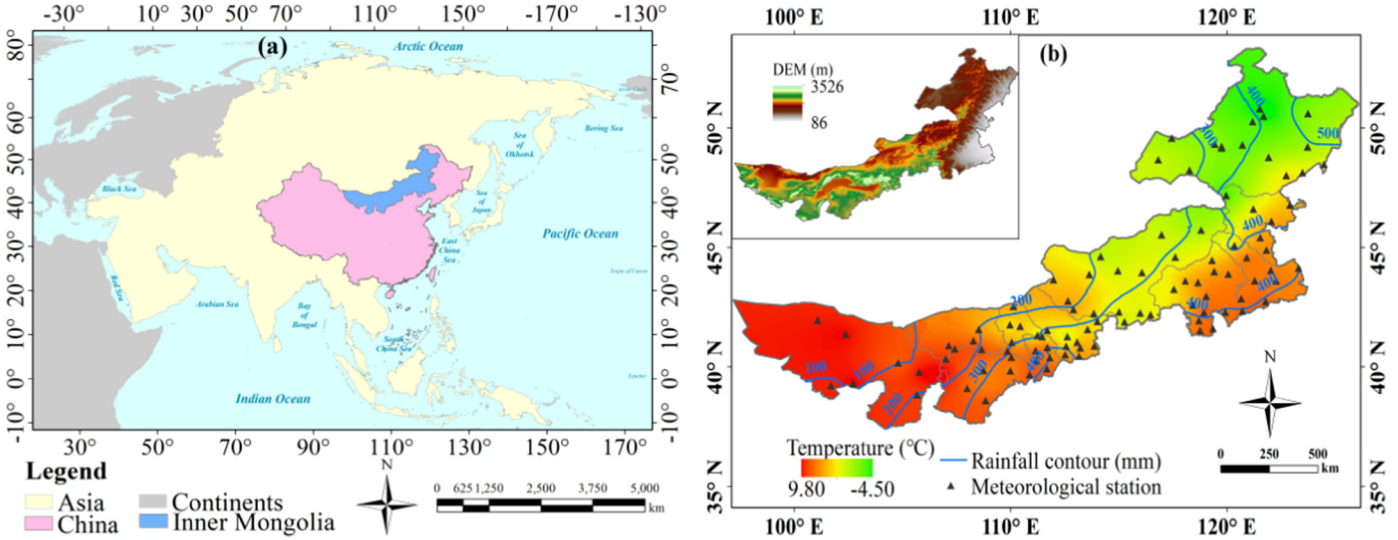

Fig. 1. Geographical location of the study area (a) and weather stations (b), and the spatial distributions of annual mean temperature and precipitation, and elevation (b).

outliers in the daily climate data and has proved to be the most effective method for data quality control used in previous studies (Zhang et al., 2005; You et al., 2010; Aguilar et al., 2005; Mark et al., 2006). After data quality control, 100 stations were maintained to study the variation in extreme climate events in Inner Mongolia; the locations of the meteorological stations are shown in Fig. 1b.

2.3. Definition of extreme indices

In this study, 14 extreme climate indices, including 8 extreme temperature indices and 6 extreme precipitation indices (Table S1), were selected from the core indices recommended by the CCI/CLIVAR/JCOMM Expert Team on Climate Change Detection and Indices (ETCCDI, http://etccdi.pacificclimate.org/). These selected indices were calculated using RClimDex V1.0 software. The frost days (FD0), cold days (TX10p), cold nights (TN10p), and cold spell duration indicator (CSDI) reflected extreme low temperature events (cold extremes), and the summer days (SU25), warm days (TX90p), warm nights (TN90p), and warm spell duration indicator (WSDI) indicated extreme high temperature events (warm extremes). The extreme precipitation indices included the maximum 1-day precipitation (RX1day), the maximum 5-day precipitation (RX5day), the number of heavy precipitation days (R10), very wet days (R95p), consecutive wet days (CWD), and consecutive dry days (CDD). Of these, the RX1day and RX5day represented extreme precipitation over a short period, which had the greatest significance in the occurrence of flood and waterlogging disasters.

2.4. Large-scale atmospheric circulation

A Pearson's correlation analysis was applied to atmospheric circulation and climate extreme indices to study the impact of atmospheric circulation types on climate extremes in Inner Mongolia, based on the potential factors affecting the climate in northern China (Deng et al., 2014; Huang et al., 2014; You et al., 2013). The large-scale oceanic-atmospheric circulation indices selected in this study included ENSO (downloaded from http://www.cpc.ncep.noaa.gov/), AO (http://www.cpc.ncep.noaa.gov/), NAO (http://ljp.gcess.cn/dct/page/1), IOD (http://www.jamstec.go.jp/frsgc/research/d1/iod/index.html), PDO (http://www.esrl.noaa.gov/psd/data/correlation/pdo.data), and the East Asian summer monsoon index (EASM) (http://ljp.gcess.cn/dct/page/1). To quantify the changes in large-scale atmospheric circulation, monthly mean geopotential height (500 hPa), winter air temperature, and summer wind fields and precipitation during 1960–2017 were derived from the NCEP/NCAR reanalysis data (http://www.cdc.noaa.gorv/). In addition, the low cloud cover data at 12:00 and 00:00 were derived from the ERA-20CM dataset (http://apps.ecmwf.int) to examine the influence of low cloud cover on extreme temperature indices.

2.5. Linear trend analysis

Linear trend analysis was used to study the spatial and temporal trends in extreme temperature and precipitation indices:

$$y = ax + b \tag{1}$$

where y is the annual index's value from 1960 to 2017; x is the year from 1960 to 2017; and a and b are the intercept and slope of the index, respectively, the latter calculated by the least square method (Eq. (2)):

$$\text{slope} = \frac{\sum_{i=1}^{n}(x_i-\overline{x})(y_i-\overline{y})}{\sum_{i=1}^{n}(x_i-\overline{x})^2} \tag{2}$$

where n is the number of years (equal to 58 in this study), denoting the year (=1, 2, 3, … 58); x_i represents the annual extreme temperature or precipitation index value in the i th year; and x_i is the multiyear average value of the index. A positive slope indicates an upward trend; otherwise, the trend in the index is downward (Zhao et al., 2012). The F test was used to determine whether or not the change was significant. The significance test can only determine the confidence level of changes and is not related to the speed of changes. The F test was calculated as follows:

$$F = U \times \frac{n-2}{Q} \tag{3}$$

where $U = \sum_{i=1}^{n}(\hat{y}i-\overline{y})^2$ is the sum of error square; $Q = \sum_{i=1}^{n}(y_i-\hat{y}i)^2$ is the regression sum of squares; y_i is the value of annual extreme temperature or precipitation index in the i th year and $\hat{y}i$ is its regression value; $\overline{y}$ is the average value of annual extreme temperature or precipitation index in 58 years ($n = 58$ in this paper). In addition, significance levels of 0.01 and 0.05 are used.

2.6. Detrended fluctuation analysis (DFA)

Detrended fluctuation analysis (DFA) is a long-range power law correlation analysis method proposed by Peng et al. (1994) for the study of DNA, but it is also suitable for nonstationary time series. After continuous development, the DFA has been widely used in the study of long-range correlation of natural systems (Li and Zhang, 2007; Varotsos et al., 2006). In recent years, researchers have used DFA to analyze the trends and extreme values in climatological and hydrological sequences (Fraedrich and Blender, 2003; Monetti et al., 2003). In this study, DFA was used to predict future development trends in extreme climate indices. It is calculated as follows:

For a temperature or precipitation sequence $\{x_k, k = 1,2,\ldots,N\}$, N is the length of the sequence, $\overline{x}$ is the average value, and the accumulative deviation sequence of the original sequence is established by:

$$y(i) = \sum_{k=1}^{N}(x_k-\overline{x}) \quad (i = 1,2,\ldots,N) \tag{4}$$

Then, the new sequence $y(i)$ is divided into N_s nonoverlapping subintervals with a length of s:

$$N_s = int(N/s) \tag{5}$$

Because the sequence is not precisely divisible, to ensure the integrity of the information, it was divided once again in the reverse direction, so that a total of $2N_s$ subintervals could be obtained. The value of s was selected according to the length of the sequence and the operation requirements.

Polynomial fitting was performed on the data of each subinterval v (v = 1, 2, …$2N_s$), and a local trend function $y_v(i)$ was obtained. We then eliminated the trend of the original sequence in the subfunction and filtered the trend out the sequence as $y_s(i)$:

$$y_s(i) = y(i)-y_v(i) \quad (i = 1,2,\ldots,N) \tag{6}$$

$y_v(i)$ can be a first order, second order, or higher order polynomial; the second-order polynomial is used here.

After the elimination of the trend, the variance in each interval was calculated as follows:

$$F^2(v,s) = \frac{1}{s}\sum_{i=1}^{s}\{y[(v-1)s+i]-y_v(i)\}^2 \quad (i = 1,2,\ldots,N_s) \tag{7}$$

$$F^2(v,s) = \frac{1}{s}\sum_{i=1}^{s}\{y[N-(v-N_s)s+i]-y_v(i)\}^2 \quad (i = N_s+1, N_s+2,\ldots,2N_s) \tag{8}$$

The second-order wave function of the whole sequence was determined as follows:

$$F(s) = \sqrt{\frac{1}{2N_s}\sum_{v=1}^{2N_s} F^2(v,s)} \quad (9)$$

Power-law correlations of F(s) and s changes were analyzed:

$$F(s) \sim s^a \text{ or, } \ln F(s) = a \ln s + b \quad (10)$$

That is, in the double logarithmic coordinate, the data were fitted by the least square method and the slope (a) of the linear trend is the scaled DFA index.

If a = 0.5, then the sequence is a random sequence and is an independent random process. If 0 < a < 0.5, then the values of the sequence are not independent and there is short-range correlation or antipersistence, which indicates the time series has the opposite trend relative to that of the previous time series. However, if 0.5 < a < 1, then the process is continuous and the future trend is consistent with the previous trend. The closer the value is to 1, the greater the tendency of this consistency. When a = 1, the sequence is a 1/f process, i.e., a nonstationary random process with 1/f spectrum, characterized by scale invariance and long-term correlation. If a ≥ 1.5, the sequence is a brown noise sequence.

In addition, the Mann-Kendall test was used to detect the abrupt change in extreme temperature and precipitation indices (Yang et al., 2017; Smadi and Zghoul, 2006). Cross wavelet transform was used to reveal the time-frequency transformation relationship between the atmospheric circulation index and extreme climate indices (Zanchettin et al., 2013).

3. Results

3.1. Variations in extreme temperature events

The temporal variation in regionally averaged annual extreme temperature events in Inner Mongolia during 1960–2017 is shown in Fig. 2 (a–h). Fig. 2 shows that the cold indices, such as FD0, TX10p, TN10p, and CSDI, significantly decreased ($p < 0.01$) at rates of −3.86 d/10 yrs, −1.88 d/10 yrs, −4.58 d/10 yrs and −1.04 d/10 yrs, respectively, from 1960 to 2017 (Fig. 2a, b, c, and d). Additionally, the decadal average values were the largest in the 1960s and the smallest in the 2000s. The average decadal value consistently decreased from the 1960s to the 2000s, and then slightly increased in the 2010s. However, the warm indices, such as SU25, TX90p, TN90p and WSDI, significantly increased at rates of 3.11 d/10 yrs, 2.06 d/10 yrs, 3.73 d/10 yrs and 0.93 d/10 yrs, respectively, over the period of 1960 to 2017 (Fig. 2e, f, g, and h). The average decadal values in SU25, TN90p, TX90p, and WSDI were the largest in the 2000s. SU25 and TN90p values were smallest in the 1970s and the 1960s, respectively. TX90p and WSDI values were smallest in the 1980s.

We also found that the cold days and nights indices (TX10p and TN10p) decreased, and the warm days and nights indices (TX90p and TN90p) increased; however, the rate of decrease in TN10p (−4.58 d/10 yrs) was larger than that in TX10p (−1.88 d/10 yrs), and the rate of increase in TN90p (3.73 d/10 yrs) was larger than that in TX90p (2.06 d/10 yrs), which indicates that the nighttime warming was higher than daytime warming. Overall, the frequency of extreme events related to low temperatures in the study area significantly decreased, while the extreme events associated with high temperatures significantly increased. This shows that extreme temperatures in Inner Mongolia have increased significantly, which is consistent with expected results of global climate warming.

Fig. S1 shows the abrupt change in extreme temperature indices based on the Mann-Kendall statistical test. It can see from figure that the cold extreme indices, FD0, TX10p, TN10p and CSDI, have obvious abrupt changes at 1989, 1994, 1985 and 1981, respectively; the warm extreme indices, SU25, TX90p, TN90p and WSDI, have obvious abrupt changes at 1999, 1993, 1989 and 1992, respectively (Fig. S1). In addition, the cold extremes have a significant decreasing trend after the abrupt change year, while the warm extremes have a significant increasing trend. These results indicate that the increasing trend of temperature is obvious in the Inner Mongolia after abrupt change.

The spatial distribution patterns for extreme temperature events are shown in Fig. 3(a–h). For the cold extremes, the region of FD0 had a decreasing trend, and its variation rate ranged from approximately −5.27 to −1.03 d/10 yrs. Of 100 stations, 95 have significantly decreased at the 0.05 significance level, and the decreasing trend gradually increased from the east to west in the study area (Fig. 3a). TX10p varied between −3.09 to −2.71 d/10 yrs, and 97% of stations showed a significant decrease; the largest change occurred in the northeast corner, and the eastern region exhibited a moderate change (Fig. 3b). The trend in TN10p changed from approximately −6.38 to −1.45 d/10 yrs, with a significant decrease in 96% of the stations; the central part of the study area had the lowest rate of decrease, and the eastern region had the smallest rate of decrease (Fig. 3c). The variation in the CSDI ranged from −2.13 to −0.12 d/10 yrs, and the stations with a significant decrease accounted for 63% of the total stations and were distributed in the middle and eastern area (Fig. 3d).

As for the warm extremes, the number of summer days (SU25) increased over the whole region, with the rate of increase ranging from 1.48 to 4.26 d/10 yrs and increasing from west to east (Fig. 3e). The rate of change in the TX90p, TN90p, and WSDI indices increased from east to west in the study area, and the southeast regions have the smallest rate; the rate of change in these indices ranged from 1.43 to 2.84, 0.98 to 5.38, and 0.24 to 1.93 d/10 yrs, respectively (Fig. 3f, g, and h). The stations exhibiting a significant increase were much larger than those exhibiting an insignificant increase. Generally, the cold extremes decreased and the warm extremes increased in the study area; the temperature in Inner Mongolia increased to a greater degree in the western region than in the eastern region.

3.2. Variations in extreme precipitation events

The regional annual series of extreme precipitation indices are shown in Fig. 4. The figure shows that the RX1day, RX5day, R95p, and CWD indices insignificantly decrease at rates of −0.16 d/10 yrs, −0.37 d/10 yrs, −0.47 d/10 yrs, −0.01 d/10 yrs, respectively, and the CCD index significantly decreased ($p < 0.01$). R10 had an insignificant slight increase (slope = 0.01) from 1960 to 2017 in the study area (Fig. 4c). These results indicate that the precipitation in the study area had no clear change over the past 58 years. In the 1990s, the RX1day, RX5day, R10, R95p, and CWD indices had the largest decadal average values, and their lowest values occurred in the 2000s. Combined with the analysis of extreme temperature indices, we found that the climate in Inner Mongolia was wet in the 1990s and dry in the 2000s.

Fig. S1 shows that there are some intersection points of UF and UB in extreme precipitation indices, but the increase or decrease of UF curve following the intersection does not exceed the critical level (Yang et al., 2017). Therefore, unlike extreme temperature indices, the variation in extreme precipitation indices in Inner Mongolia is relatively complex, and there is no obvious abrupt change over the past 58 years (Fig. S1).

Fig. 5 shows the spatial distribution of variation in extreme precipitation indices. The RX1day tendency rate ranged from −1.23 to 0.83 d/10 yrs. The northeast and western region has an increasing trend, and the other regions have decreasing trends; 54% of stations had a decreasing trend and 46% had an increasing trend (Fig. 5a). The RX5day tendency rate ranged from −3.72 to 3.67 d/10 yrs, with 42% of stations exhibiting an increasing trend distributed northeast and west of study area, and the rest of the stations in the other regions

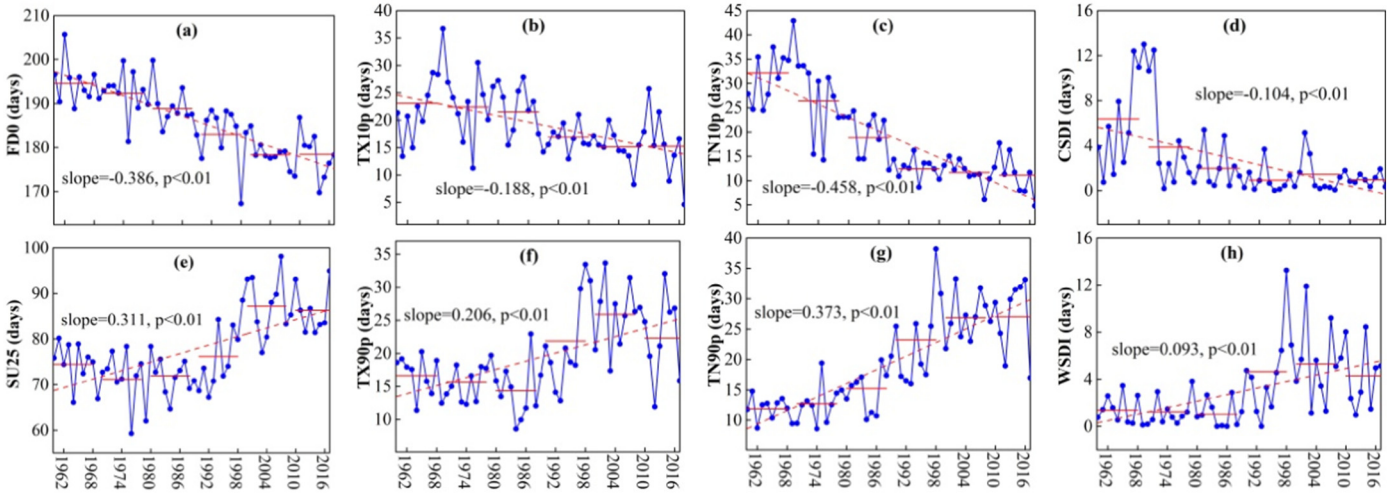

Fig. 2. Linear regression trends for regional annual extreme temperature indices (a) FD0, (b) TX10p, (c) TN10p, (d) CSDI, (e) SU25, (f) TX90p, (g) TN90p, and (h) WSDI in Inner Mongolia during 1960 to 2017 (the blue line is the annual series of the considered index, the dashed red line is the linear trend, and the red line is the average value for each decade).

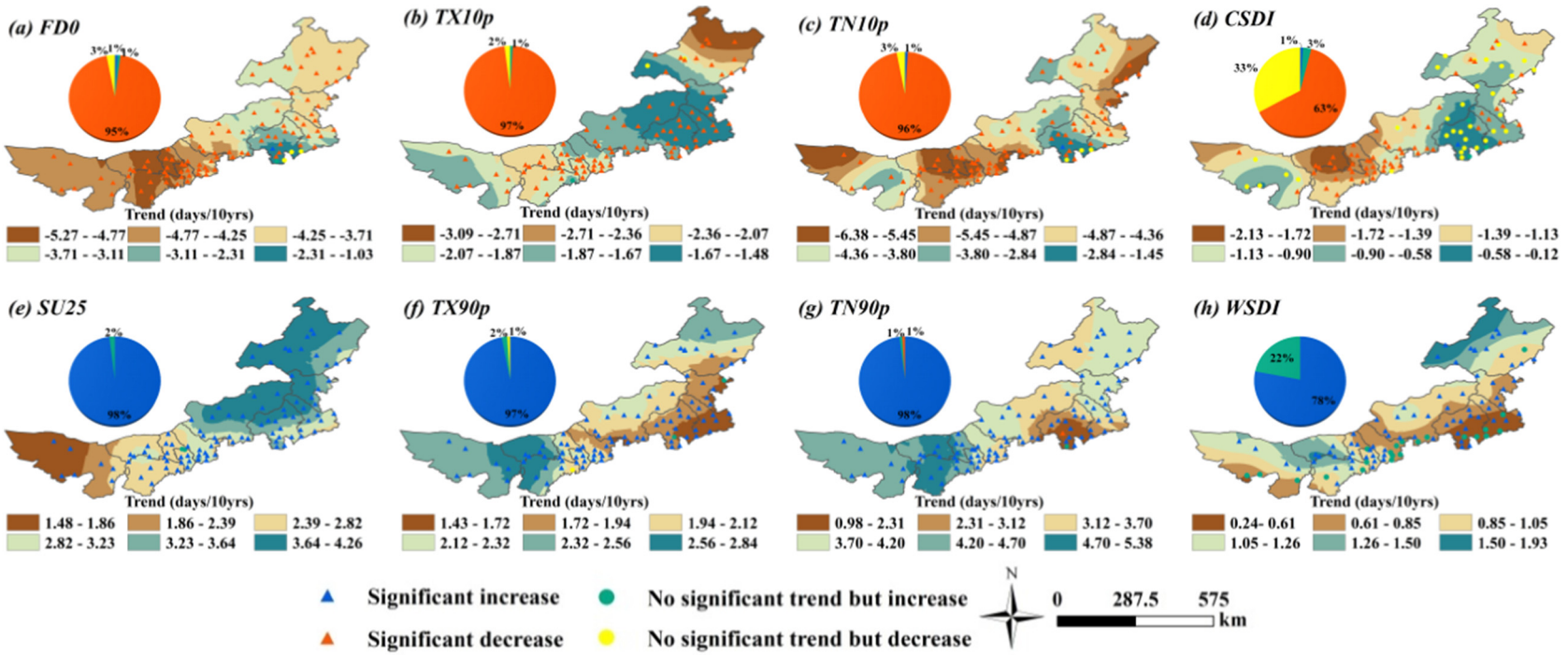

Fig. 3. Spatial patterns of decadal trends in indices of extreme temperature events over Inner Mongolia during 1960–2017.

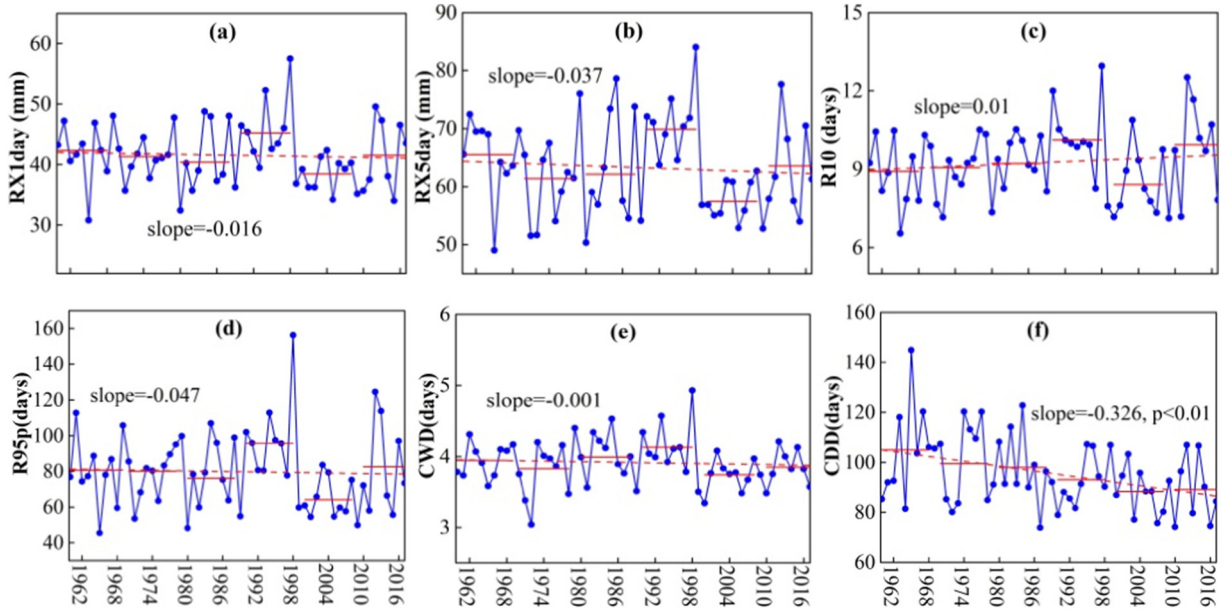

Fig. 4. Linear regression trends for regional annual extreme temperature indices (a) RX1day, (b) RX5day, (c) R10, (d) R95p, (e) CWD, and (f) CDD in Inner Mongolia during 1960 to 2017 (the blue line is the annual series of the selected index, the dashed red line is the linear trend, and the red line is the average value in each decade).

exhibiting a decreasing trend (Fig. 5b). R10 ranged from −0.15 to 0.38 d/10 yrs, with 66% of stations having an increasing trend, while a decreasing trend appeared in the mid-eastern region (Fig. 5c). The trend in R95p ranged from −5.57 to 5.92 d/10 yrs, with the northeast and southwest regions exhibiting increasing trends (Fig. 5d). CWD varied between −0.08 and 0.04 d/10 yrs, and 54% of stations showed a decrease, with a larger decrease occurring in the central-east region of the study area (Fig. 5e). The rate of CDD ranged from −7.47 to 0.73 d/10 yrs, with 87% of stations showing a decrease which was most significant in the middle and eastern regions (Fig. 5f).

The trends in the extreme precipitation indices vary spatially, which illustrates the inhomogeneity of rainfall in the area. The changes in extreme precipitation indices for the whole region have similar trends; that is, most indices in the northeast and western regions have an increasing tendency, while most indices in the central-east region have

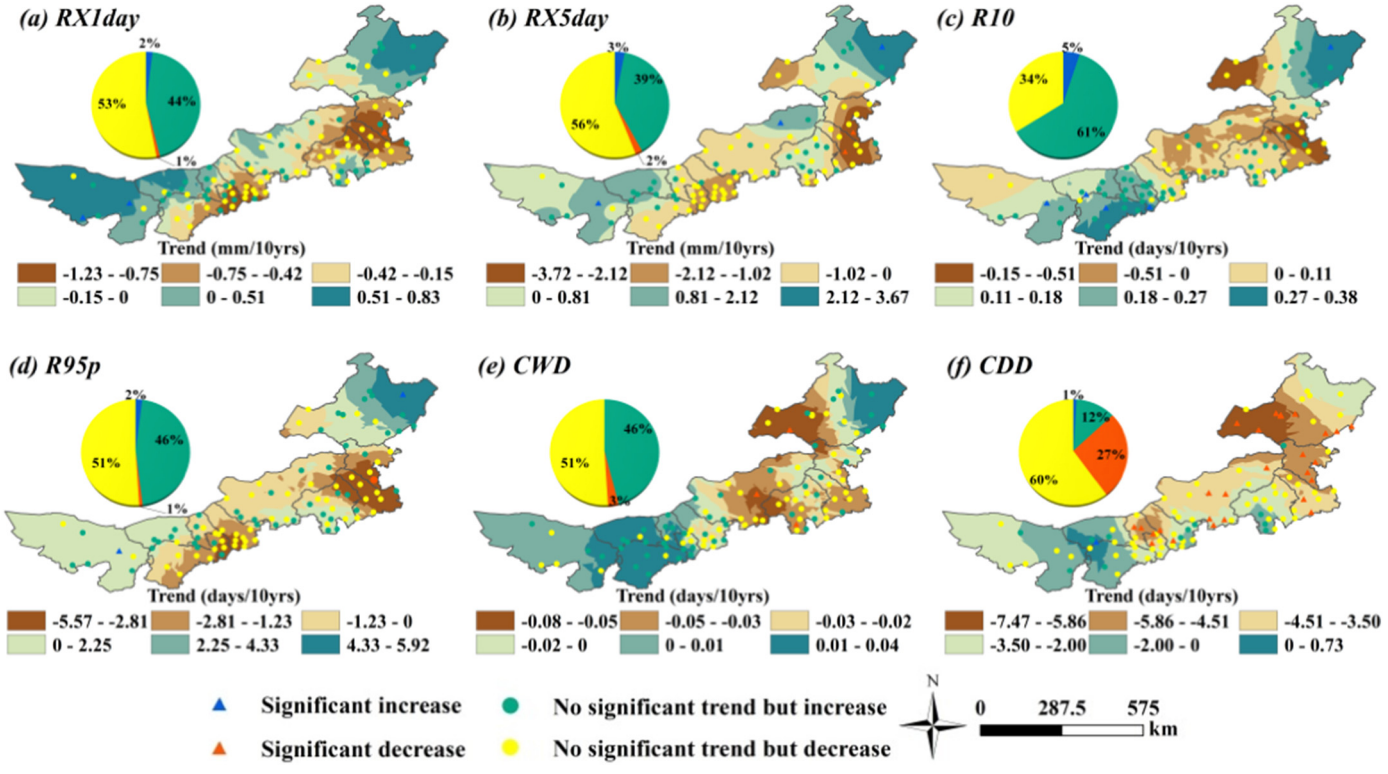

Fig. 5. Spatial patterns of decadal trends in indices of extreme precipitation events over Inner Mongolia during 1960–2017.

larger decreasing trends. In addition, the number of stations with decreasing trends exceeded those with increasing trends.

3.3. Long-range correlation analysis based on DFA

To study the changing trends in future extreme temperature and precipitation events, a long-range correlation was conducted based on DFA, and the results are shown in Fig. 6(a–n). The figure shows that the DFA scaling exponent *a* in FD, TX10p, TN10p, CSDI, SU, TX90p, TN90p, and WSDI was 0.611, 0.669, 0.662, 0.689, 0.635, 0.667, 0.618, and 0.583, respectively (Fig. 6a–h). Because $0.5 < a < 1$, the values of each sequence were not independent, and all had long-range correlation, indicating that the future trend in each extreme temperature index is consistent with the change in trend over the past 58 years (1960–2017). That is, the cold extremes (FD0, TX10p, TN10p, and CSDI) will continue to decrease and the warm extremes (SU25, TX90p, TN90p, and WSDI) will continue to increase, as indicated by previous analyses.

For the extreme precipitation indices, the DFA scaling exponent *a* in RX1day, RX5day, R10, R95p, CWD, and CDD was 0.539, 0.547, 0.616, 0.543, 0.568, and 0.714, respectively (Fig. 6i–n). This indicates that the future trend in each extreme precipitation index is consistent with the change in trend over the past 58 years; that is, these indices will exhibit decreasing trends in the future. The closer the DFA index value is to 1, the greater the rate of decrease; therefore, CDD will be consistent with the original trend for a longer period. We also found that the DFA exponent values in extreme temperature indices were generally larger than those in the extreme precipitation indices, which implies that the future trends in temperature indices have a stronger long-range correlation with the current state compared to the future trends in precipitation indices.

3.4. Correlation between extreme temperature and precipitation events

Table 1 shows the correlation between extreme temperature and extreme precipitation indices. The table shows that there was a significant correlation between the extreme temperature indices ($p < 0.01$). The warm extremes were significantly negatively correlated with cold extremes, while the warm extremes and cold extremes were positively correlated with each other. For example, the frost days had a positive correlation with cold extremes and had a negative correlation with warm extremes. In addition, statistically significant positive correlations existed between the extreme precipitation indices, except for CDD.

The extreme precipitation indices were generally positively correlated with cold extremes and negatively correlated with warm extremes, but not with significance (except for the significant correlation of SU25 with precipitation indices, and CDD with FD0, TN10p and TN90). This correlation indicates that the decrease in cold extremes and the increase in warm extremes reduced the possibility of extreme precipitation events (Figs. 2, 4).

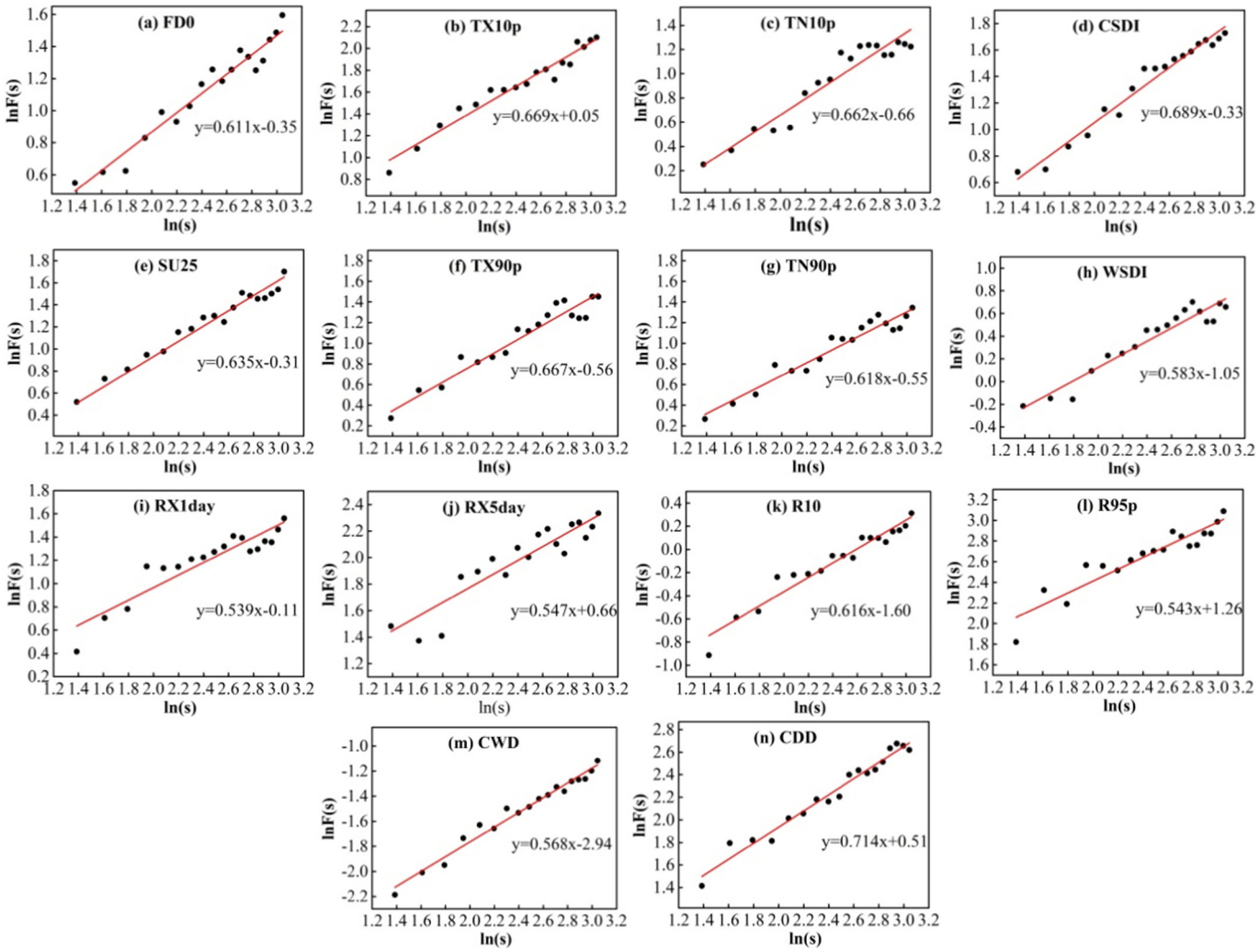

Fig. 6. DFA long-range forecasting of extreme temperature and precipitation indices.

Table 1
The Pearson's correlation between extreme temperature and extreme precipitation indices. (*significant at the 0.05 level; **significant at the 0.01 level.)

Index	FD0	TX10p	TN10p	CSDI	SU25	TX90p	TN90p	WSDI	RX1day	RX5day	R10	R95p	CWD	CDD
FD0	1													
TX10p	0.616**	1												
TN10p	0.792**	0.783**	1											
CSDI	0.412**	0.682**	0.735**	1										
SU25	−0.489**	−0.537**	−0.466**	−0.283*	1									
TX90p	−0.628**	−0.537**	−0.511**	−0.337*	0.698**	1								
TN90p	−0.866**	−0.632**	−0.784**	−0.460**	0.687**	0.848**	1							
WSDI	−0.562**	−0.391**	−0.455**	−0.303*	0.551**	0.876*	0.769**	1						
RX1day	0.063	0.112	0.003	0.022	−0.301*	−0.175	−0.037	0.007	1					
RX5day	0.003	0.113	0.018	0.001	−0.330*	−0.221	−0.096	−0.031	0.909**	1				
R10	−0.250	0.059	0.181	−0.080	−0.356**	−0.167	0.109	0.001	0.696**	0.707**	1			
R95p	0.080	0.142	−0.013	−0.023	−0.338*	−0.205	−0.021	−0.005	0.916**	0.864**	0.863**	1		
CWD	−0.102	0.118	−0.091	0.011	−0.386**	−0.147	−0.034	0.033	0.456**	0.642**	0.572**	0.536**	1	
CDD	0.296*	0.250	0.382**	0.172	−0.204	−0.200	−0.373**	−0.161	−0.091	−0.058	−0.197	−0.059	0.142	1

The red frame contains the correlation coefficiect between extreme temperature and precipitation.

3.5. Teleconnection relationship between extreme climate events and large-scale atmospheric circulation

As representative indices of the typical atmospheric circulation changes in the northern hemisphere, the six selected indices represent the characteristics of the atmospheric circulation in different regions, but they jointly affect the distribution of extreme climate events in the northern hemisphere. Fig. 7 demonstrates the Pearson's correlation coefficients between extreme temperature and precipitation indices and atmospheric circulation indices in Inner Mongolia during 1960–2017. There was a significant positive correlation between ENSO and warm extremes, a significant negative correlation between ENSO and cold extremes, and no significant negative correlation between ENSO and extreme precipitation indices, which indicates that ENSO had a significant impact on extreme temperature events in Inner Mongolia. The AO had a significant negative correlation with cold

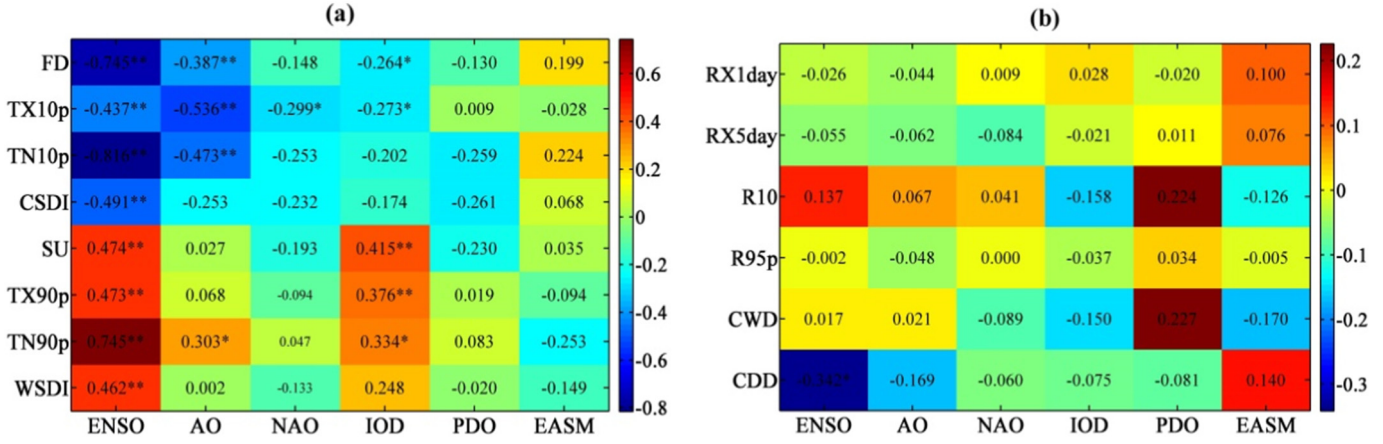

Fig. 7. Pearson's correlation coefficients between extreme temperature and precipitation indices and atmospheric circulation indices in Inner Mongolia during 1960–2017. (*significant at the 0.05 level; **significant at the 0.01 level.)

extremes, and an insignificant positive correlation with warm extremes. The NAO had a negative correlation with temperature events and had a higher correlation with cold extremes than with warm extremes. The IOD had a significant positive correlation with warm extremes and had a negative correlation with cold extremes. The PDO and EASM had weak and insignificant correlations with temperature extremes (Fig. 7a). The six selected atmospheric circulation indices have no significant influence on extreme precipitation indices (Fig. 7b).

Fig. S2 shows the spatial distribution of the correlation between extreme temperature and precipitation indices and atmospheric circulation indices in Inner Mongolia, which clearly shows the spatial influence of atmospheric circulation on the extreme climate events in Inner Mongolia. Combined with Fig. S3, it can be concluded that the areas of positively correlated with atmospheric circulation indices were larger than those with negative correlations in the warm extremes. In addition, the areas of cold extremes had negative correlations with atmospheric circulation indices were larger than those with positive correlation. Spatial correlation analysis between extreme precipitation events and atmospheric circulation showed that these factors did not have significant positive or negative correlation in Inner Mongolia.

Because the impact of the large-scale atmosphere index on extreme temperature and precipitation indices is reflected mainly on the interdecadal scale, the relationship between atmospheric indices FD0, SU25, RX5day and R95p was analyzed by cross wavelet transform. As demonstrated by the correlation analysis, the influence of the atmospheric indices on the 4 cold extremes and 4 warm extremes is consistent but has no significant impact on the precipitation indices. Therefore, we choose FD0 (cold extremes), SU25 (warm extremes), RX5day and R95p as the representative indices used to reveal the time-frequency relationship with atmospheric indices.

Fig. 8 shows the cross-wavelet transform of ENSO and extreme indices. The figure shows a significant resonance cycle of 1–3 years during 1971–1978 and 3–5 years during 1990–2000 occurred between ENSO and FD0. The change in the phase angle proves that FD0 lagged behind ENSO in the first cycle, and the two series showed an anti-phase resonance in the second frequency band, indicating a negative correlation between ENSO and FD0 (Fig. 8a). Fig. 8(b) shows that ENSO and SU25 have significant resonance cycles of one to four years during 1972–1980 and 1991–1998; SU25 was ahead of ENSO in the first cycle and was positively correlated with ENSO in the second cycle. Resonance cycles of 2–6 years during 1967–1974 and 1986–1990, and 4–6 years during 1975–1985, occurred between NESO and RX5day; RX5day was ahead in three cycles (Fig. 8c). A significant resonance cycle of 1–4 years occurred during 1965–1975 between ENSO and R95p, and the change in the phase angle indicates that R95p was ahead in this cycle (Fig. 8d). We can also see from Fig. S4 that IOD and the extreme climate indices have significant resonance cycles.

4. Discussion

We analyzed the temporal and spatial evolution of extreme climate events in Inner Mongolia during 1960–2017 by selecting indices of extreme temperature and precipitation events and explored their relationship with large-scale atmospheric circulation. On the one hand, nighttime warming was higher than daytime warming, and the increase in extreme low temperature indices was larger than that in extreme

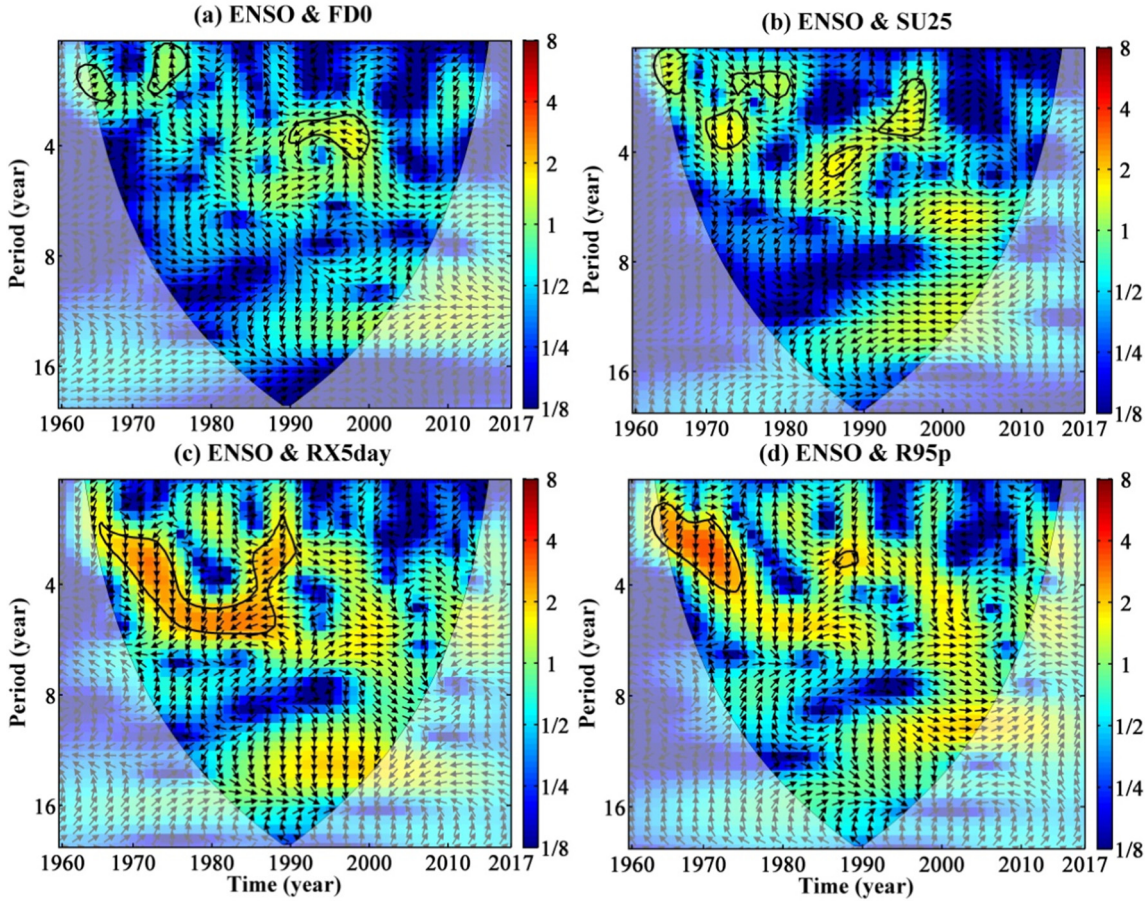

Fig. 8. Cross-wavelet transforms of ENSO and FD0 (a), ENSO and SU25 (b), ENSO and RX5day (c), ENSO and R95p (d) time series. (The thick black contours depict the 5% confidence level, and the black line is the cone of influence. Right-pointing arrows indicate that the two signals are in phase, while left-pointing arrows indicate anti-phase signals; down-pointing arrows indicate that the extreme indices are ahead of the atmospheric index, while up-pointing arrows indicate that the extreme indices lag behind the atmospheric index.)

high temperature indices, which is consistent with research conducted by Chen and Zhao (2017). The main reason for this change is that there is a larger magnitude of warming in winter than in summer (Bao et al., 2010), and the radiative forcing effect of greenhouse gases in winter can also cause significant air warming (Aguilar et al., 2009). On the other hand, the rate of change in extreme indices in western Inner Mongolia desert areas was large, while the rate of change in eastern Inner Mongolia forest areas was small. This may be related to the forest's ability to store carbon and mitigate climate change (Lu et al., 2009), while severe land use change and frequent human activities profoundly affect the climate in desert areas (Connolly, 2004). The change in regional land use and land cover has an influence on climate (John et al., 2009).

In the context of global warming, unlike the extreme temperature events, the decrease in variation of extreme precipitation events over the last 58 years in Inner Mongolia was not significant, but clear differences were observable at a large spatial scale, consistent with previous observations (You et al., 2011). The characteristics of regional precipitation changes may be influenced by the unique cyclical nature of each atmospheric circulation (Li et al., 2015). The study of Si et al. (2012) showed that the extreme low temperature events in Inner Mongolia have the same trend as that of the AO, the subtropical high and westerly circulation. Li et al. (2015) found that the change in precipitation in Inner Mongolia has a strong relationship with the Northern boundary of WASMR, which moved southward because of the enhanced westerlies, and that the regional precipitation cycles may be influenced by their own periods of NAO and PDO. ENSO, NAO and SO have been found to have significant correlations with temperature changes in northern southern China (Wan et al., 2010; Gong et al., 2009), consistent with our results.

We also found that there have been significant abrupt changes in extreme temperature indices, although the point at which these changes take place is different for different indices, and after the change, the indices have either significantly increased or decreased, and the atmospheric circulation indices have significantly impacted the extreme temperature and precipitation events. Therefore, to quantify the changes in large-scale atmospheric circulation, we calculated the mean circulation composites and then investigated the role of circulation change on the trends in extreme climate events. First, we detected the abrupt change point of annual mean temperatures during 1960–2017 in Inner Mongolia and found that the annual mean temperature has a significant turning point in 1993 (Fig. 9). Then, the change in circulation in the two periods before and after the abrupt change was calculated by subtracting 1960–1993 from 1994 to 2017 based on the NCEP/NCAR and ERA-20CM reanalysis data.

As shown in Fig. 10(a), the larger variation in the monthly mean geopotential height (500 hPa) occurred in summer (>30 gpm) in Mongolia (near 45°N and 100°E), and a Eurasian continent anticyclone centered on Mongolia was formed. In addition, a cyclone also appeared in the western Pacific (near 40°N and 140°E), which indicated a weaker eastern Asian summer monsoon during 1994–2017. Inner Mongolia also contains areas with large geopotential height differentials and is located under the anticyclone centered on Mongolia, which is disadvantageous for the formation of rain. The intensification of the northeasterly winds reduced the northern and eastern extent of the westerly jet stream and southwesterly flow from the ocean. This caused the decrease in the annual precipitation and extreme precipitation events in Inner Mongolia (Fig. 10d).

As shown in the geopotential height composite, an enhanced anticyclonic circulation occurred in Mongolia and Inner Mongolia near 40°N and 125°E (Fig. 10b). Additionally, the southwesterly wind in northern Mongolia was strengthened, which reduced the extent of the winter monsoon in the south and decreased the incursions of colder air, leading to warming in the region in winter (Fig. 10c).

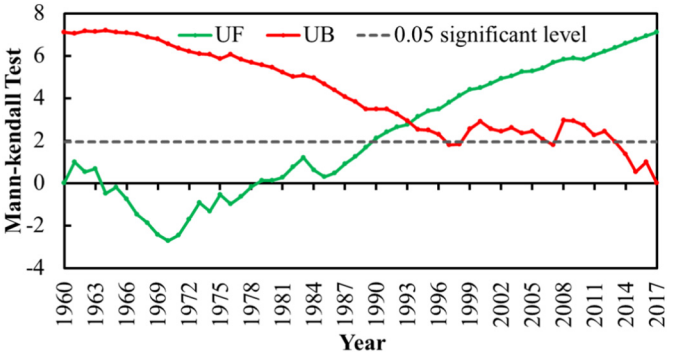

Fig. 9. MK abrupt change detection for the annual mean temperature during 1960–2017. The green and red solid lines represent the progressive series, UF, and the retrograde series, UB. Horizontal dashed lines are the confidence limits (0.05).

Fig. 10(e) and (f) show the difference in daytime and nighttime cloudiness between 1994–2017 and 1960–1993. The daytime cloudiness decreased overall, and the few clouds in the daytime will lessen the weakening effect of atmosphere on solar radiation, and this will enhanced the warming. Thus, the number of warm days increased and the number of cold days decreased; the increase in nighttime cloudiness caused an increase in the atmospheric counter radiation and had a heat preservation effect on the ground. Resulting the warming was significant and showed an increase in the number of warm nights and a decrease in the number of cold nights. This is consistent with the results of the previous analysis.

Moreover, the extreme temperature events in Inner Mongolia greatly increased, but the precipitation decreased. This will inevitably increase the need for fire protection of forests and grasslands. The decreases in extreme low temperature events will not only help the vegetation overwinter but will also help the pests overwinter and will increase the risk of pest disease in the region (Jia, 2012). Human activities also play an important role in extreme climate change; the unreasonable use of water resources, land resources, and forest resources will further change the regional climate (Zhao et al., 2016; Yan et al., 2014). In the future, we should focus on analyzing the role of human activities in regional climate warming, increase the in-depth study of the mechanisms of extreme climate events, and ensure adequate prevention and monitoring to better provide a decision-making basis for regional agricultural and animal husbandry production.

5. Conclusion

In this study, 14 indices of extreme temperature and precipitation events were selected. The spatial and temporal changes from 1960 to 2017 were analyzed based on linear trend analysis, and their teleconnections to large-scale atmospheric circulation in Inner Mongolia were explored. This work led to the following main conclusions:

(1) Extreme high temperature indices have significantly increased, while the extreme low temperature indices have significantly decreased; and both kinds of indices have obvious abrupt changing points. In addition, the warming at night was higher than the warming in the daytime. The temperature in Inner Mongolia increased, and the increase in the western region was larger than that in eastern region.
(2) The extreme precipitation indices in Inner Mongolia did not show significant changes during 1960–2017. At a broad spatial scale, the northeast and western regions have an increasing tendency, while most indices in the central-east region had larger decreasing trends.

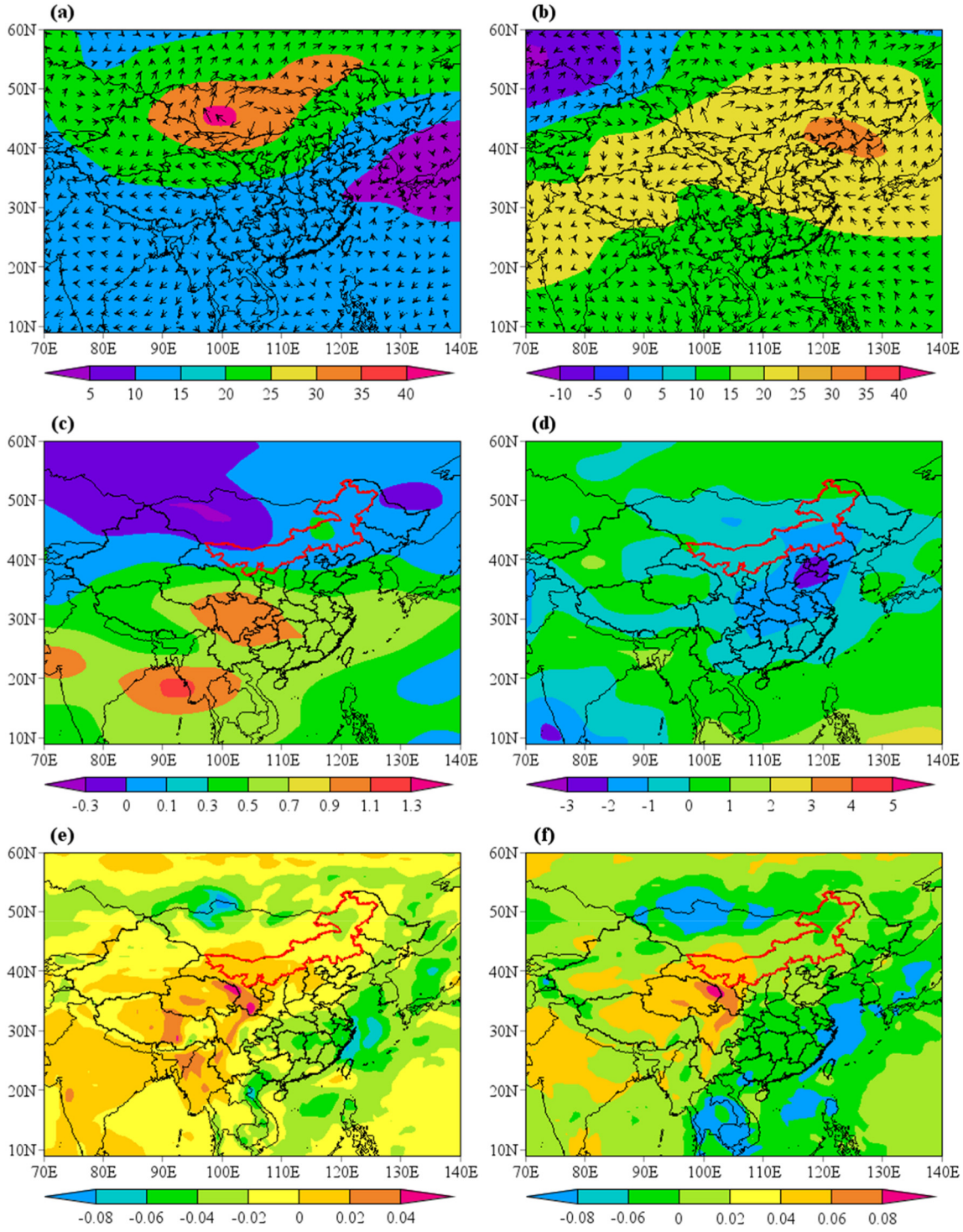

Fig. 10. Differences in geopotential height and wind speed in summer (a) and winter (b), air temperature in winter (c), precipitation in summer (d), and annual mean daytime (e) and nighttime cloudiness (f) at 500 hPa between 1994–2017 and 1960–1993.

(3) Correlation between extreme temperature and precipitation events showed that the extreme precipitation indices were generally insignificantly positively correlated with cold extremes and were negatively correlated with warm extremes.
(4) The extreme temperature and precipitation indices had long-range correlation based on DFA, indicating that the extreme climate indices will continue to maintain their current trend direction in the future.
(5) The atmospheric circulation indices ENSO, AO, and IOD had strong positive influences on warm extremes, and had strong negative influences on cold extremes in Inner Mongolia. This indicated that the trends in extreme temperature and precipitation events partially resulted from the large-scale oscillations.
(6) Large-scale atmospheric circulation changes calculated from NCEP/NCAR and ERA-20CM reanalysis data showed that strengthening anticyclone circulation, increasing geopotential height, weakening monsoon flow, decreasing daytime cloudiness and increasing nighttime cloudiness have contributed to the changes in climate extremes in Inner Mongolia.

Acknowledgements

This study was financially supported by the National Key Technology R&D Program of China under Grant (No. 2013BAK05B01 and No. 2013BAK05B02), China Special Fund for Meteorological Research in the Public Interest (No. 2016006), the National Natural Science Foundation of China under Grant (No. 41571491, No. 41371495 and No. 61631011) and the Program of Introducing Talents of Discipline to Universities (B16011).

Appendix A. Supplementary data

Supplementary data to this article can be found online at https://doi.org/10.1016/j.scitotenv.2018.08.262.

References

Abiodun, B.J., Lawal, K.A., Salami, A.T., Abatan, A.A., 2013. Potential influences of global warming on future climate and extreme events in Nigeria. Reg. Environ. Chang. 13 (3), 477–491.
Aguilar, E., Peterson, T.C., Obando, P.R., Frutos, R., Retana, J.A., Solera, M., et al., 2005. Changes in precipitation and temperature extremes in Central America and northern South America, 1961–2003. J. Geophys. Res. Atmos. 110 (D23), 3233–3250.
Aguilar, E., Barry, A.A., Brunet, M., Ekang, L., Fernandes, A., Massoukina, M., Mbah, J., Mhanda, A., Nascimento, D.J.D., Petersion, T.C., Umba, O.T., Tomou, M., Zhang, X., 2009. Changes in temperature and precipitation extremes in western central Africa, Guinea Conakry, and Zimbabwe, 1955–2006. J. Geophys. Res. Atmos. 114 (D2), 356–360.
Alexander, L.V., Zhang, X., Petersson, T.C., Caesar, J., Gleason, B., Tank, A.M.G.K., et al., 2006. Global observed changes in daily climate extremes of temperature and precipitation. J. Geophys. Res. Atmos. 111 (D5), 1042–1063.
Anders, M., Jones, P.D., 2005. Trends in indices for extremes in daily temperature and precipitation in central and western Europe, 1901–99. Int. J. Climatol. 25 (9), 1149–1171.
Bao, Y., Li, X., Li, C., 2010. Spatial temporal distribution characteristics of temperature in Inner Mongolia during 1961–2007. J. Arid Land Resour. Environ. 24 (12), 80–84.
Bao, Y., Li, X.B., Huang, L.M., 2011. Spatial-temporal distribution characteristics of precipitation in Inner Mongolia from 1961–2007. Arid Land Geogr. 34 (1), 52–61.
Barrett, B., Charles, J.W., Temte, J.L., 2015. Climate change, human health, and epidemiological transition. Prev. Med. 70, 69–75.
Botzen, W.J.W., van den Bergh, J.C.J.M., 2009. Managing natural disaster risks in a changing climate. Environ. Hazards 8 (3), 209–225.
BrÖ, S., Nnimann, Luterbacher, J., Staehelin, J., Svendby, T.M., Hansen, G., Svenøe, T., 2004. Extreme climate of the global troposphere and stratosphere in 1940–42 related to El Niño. Nature 431 (7011), 971–974.
Brown, P.J., Bradley, R.S., Keimig, F.T., 2010. Changes in extreme climate indices for the northeastern United States, 1870–2005. J. Clim. 23 (24), 6555–6572.
Chan, J.C.L., Zhou, W., 2005. PDO, ENSO and the early summer monsoon rainfall over south China. Geophys. Res. Lett. 32 (8), 93–114.
Chen, H., Sun, J., 2015. Changes in climate extreme events in China associated with warming. Int. J. Climatol. 35 (10), 2735–2751.
Chen, J.Y., Zhao, J.B., 2017. Trends of extreme weather events in Inner Mongolia during the period of 1960–2014. Arid Zone Res. 34 (5), 997–1009.
Chen, X.Q., Peng, J.D., Li, H.M., 2009. Seasonal and regional differences of air temperature changes in Inner Mongolia. Geogr. Res. 28 (1), 27–35.
Connolly, D., 2004. Evaluating the influence of different vegetation biomes on the global climate. Clim. Dyn. 23 (3–4), 279–302.
Coumou, D., Rahmstorf, S., 2012. A decade of weather extremes. Nat. Clim. Chang. 2 (7), 491–496.
Coumou, D., Robinson, A., Rahmstorf, S., 2013. Global increase in record-breaking monthly-mean temperatures. Clim. Chang. 118 (3–4), 771–782.
Daly, C., Helmer, E.H., Quiñones, M., 2003. Mapping the climate of Puerto Rico, Vieques and Culebra. Int. J. Climatol. 23 (11), 1359–1381.
Deng, H., Chen, Y., Shi, X., Li, W., Wang, H., Zhang, S., Fang, G., 2014. Dynamics of temperature and precipitation extremes and their spatial variation in the arid region of northwest China. Atmos. Res. 138, 346–355.
Diffenbaugh, N.S., Singh, D., Mankin, J.S., Horton, D.E., Swain, D.L., Touma, D., Charland, A., Liu, Y., Haugen, M., Tsiang, M., Rajaratnam, B., 2017. Quantifying the influence of global warming on unprecedented extreme climate events. PNAS 114 (19), 4881–4886.
Ding, Y., Zhang, J., Song, Y., 2002. Weather and climate extreme affaires and its relationship with global warming. Meteorol. Mon. 28 (3), 3–7.
Douville, H., 2006. Impact of regional SST anomalies on the Indian monsoon response to global warming in the CNRM climate model. J. Clim. 19 (10), 2008–2024.
Fraedrich, K., Blender, R., 2003. Scaling of atmosphere and ocean temperature correlations in observations and climate models. Phys. Rev. Lett. 90 (10), 108501.
Gao, Y., Feng, Q., Liu, W., Lu, A., Wang, Y., Yang, J., Cheng, A., Wang, Y., Su, Y., Liu, L., Ma, Q., 2015. Changes of daily climate extremes in Loess Plateau during 1960–2013. Quat. Int. 371 (1), 5–21.
Gong, Z.Q., Wang, X.J., Zhi, R., Feng, G.L., 2009. Regional characteristics of temperature changes in China during the past 58 years and its probable correlation with abrupt temperature change. Acta Phys. Sin. 58 (6), 4342–4353.
Goovaerts, P., 2000. Geostatistical approaches for incorporating elevation into the spatial interpolation of rainfall. J. Hydrol. 228 (1), 113–129.
Hao, Z., Aghakouchak, A., Phillips, T.J., 2013. Changes in concurrent monthly precipitation and temperature extremes. Environ. Res. Lett. 8 (3), 1402–1416.
Hidalgo-Muñoz, J.M., Argüeso, D., Gámiz-Fortis, S.R., Esteban-Parra, M.J., Castro-Díez, Y., 2011. Trends of extreme precipitation and associated synoptic patterns over the southern Iberian peninsula. J. Hydrol. 409 (1–2), 497–511.
Hou, H., Yin, X., You, D., Chen, Q., Tong, G., Zheng, Y., 2008. Apocalypse of overseas of experiences on emergency anti-disaster mechanism for China power system. Autom. Electr. Power Syst. 32 (12), 89–93.
Huang, Y., Wang, H., Fan, K., Gao, Y., 2014. The western Pacific subtropical high after the1970s: westward or eastward shift? Clim. Dyn. 44 (7–8), 2035–2047.
IPCC SREX, 2012. In: Field, C.B., Barros, V., Stocker, T.F., Dahe, Q., Dokken, D.J., Ebi, K.L., Mastrandrea, M.D., Mach, K.J., Plattner, G.-K., Allen, S.K., Tignor, M., Midgley, P.M. (Eds.), Managing the Risks of Extreme Events and Disasters to Advance Climate Change Adaptation. Special Report of the Intergovernmental Panel on Climate Change. Cambridge University Press, Cambridge, United Kingdom and New York, NY, USA.
Jia, W.X., 2012. Temporal and spatial change of climate extremes in Qilian Mountains and Hexi Corridor during last fifty years. Arid Land Geogr. 35 (4), 559–567.
Jiang, D., Wang, K., Li, Z., 2011. Trends of extreme precipitation events over Shandong province from 1961 to 2008. Sci. Geogr. Sin. 31 (9), 1118–1124.
John, R., Chen, J.Q., Lu, N., Wilske, B., 2009. Land cover/land use change in semi-arid Inner Mongolia: 1992–2004. Environ. Res. Lett. 4 (4), 45010–45019.
Leonard, M., Westra, S., Phatak, A., Lambert, M., Hurk, B.V.D., McInnes, K., Risbey, J., Schuster, S., Jakob, D., Stafford-Smith, M., 2013. A compound event framework for understanding extreme impacts. WIREs Clim. Change 5 (1), 113–128.
Li, Z., Zhang, Y.K., 2007. Quantifying fractal dynamics of groundwater systems with detrended fluctuation analysis. J. Hydrol. 336 (1–2), 139–146.
Li, Z.X., He, Y.Q., Wang, P.Y., Theakstone, W.H., An, W.L., Wang, X.F., Lu, A.G., Zhang, W., Cao, W.H., 2012. Changes of daily climate extremes in southwestern China during 1961–2008. Glob. Planet. Chang. 80 (80–81), 255–272.
Li, W., Li, C., Liu, Z., Han, D., Sun, P., Jiang, H., 2015. Distribution of precipitation and its effect factors analysis in the central and western regions of Inner Mongolia during the last 60 years. J. Inn. Mong. Agric. Univ. 36 (1), 85–94.
Lu, N., Wilske, B., Ni, J., John, R., Chen, J., 2009. Climate change in Inner Mongolia from 1955 to 2005-trends at regional, biome and local scales. Environ. Res. Lett. 4 (4). https://doi.org/10.1088/1748-9326/4/4/045006.
Ma, Z.G., Fu, C.B., Ren, X.B., Yang, C., 2003. Trends of annual extreme temperature and its relationship to regional warming in Northern China. Acta Geograph. Sin. 58, 11–20.
Mark, N., Bruce, H., Stephenson, D.B., Alois, T., Andries, K., Atanasio, M., et al., 2006. Evidence of trends in daily climate extremes over southern and West Africa. J. Geophys. Res. Atmos. 111 (D14), 3007–3021.
Monetti, R.A., Havlin, S., Bunde, A., 2003. Long-term persistence in the sea surface temperature fluctuations. Phys. A 320, 581–589.
Muhire, I., Ahmed, F., Abutaleb, K., 2015. Relationships between Rwandan seasonal rainfall anomalies and Enso events. Theor. Appl. Climatol. 122 (1–2), 271–284.
Omondi, P.A., Awange, J.L., Forootan, E., Ogallo, L.A., Barakiza, R., Girmaw, G.B., et al., 2013. Changes in temperature and precipitation extremes over the greater horn of Africa region from 1961 to 2010. Int. J. Climatol. 34 (4), 1262–1277.
Pascual, A., Valero, F., Martín, M.L., Garcíalegaz, C., 2013. Spanish extreme winds and their relationships with Atlantic large-scale atmospheric patterns. Am. J. Clim. Chang. 2 (3A), 23–35.
Peng, C.K., Buldyrev, S.V., Havlin, S., Simons, M., Stanley, H.E., Goldberger, A.L., 1994. Mosaic organization of DNA nucleotides. Phys. Rev. E 49 (2), 1685–1689.
Planton, S., Déqué, M., Chauvin, F., Terray, L., 2008. Expected impacts of climate change on extreme climate events. Compt. Rendus Geosci. 340 (9), 564–574.
Rangecroft, S., Suggitt, A.J., Anderson, K., Harrison, S., 2016. Future climate warming and changes to mountain permafrost in the Bolivian Andes. Clim. Chang. 137 (1–2), 231–243.
Shea, J.M., Immerzeel, W.W., Wagnon, P., Vincent, C., Bajracharya, S., 2015. Modelling glacier change in the Everest region, Nepal Himalaya. Cryosphere 9 (3), 1105–1128.
Shi, Z.J., Gao, J.X., Xu, L.H., 2011. Effect of vegetation on changes of temperature and precipitation in Inner Mongolia, China. Ecol. Environ. Sci. 20 (11), 1594–1601.
Si, Y., Li, H., Yang, J., Yang, L., Liu, X., 2012. The circulation characteristics and predictive concept model of occurrence of extreme microtherm event in Inner Mongolia. Meteorol. J. Inn. Mong. (6), 3–9.
Smadi, M.M., Zghoul, A., 2006. A sudden change in rainfall characteristics in Amman, Jordan during the mid 1950s. Am. J. Environ. Sci. 2 (3), 84–91.
Su, Z., Hao, Z., Yuan, F., Chen, X., Cao, Q., 2017. Spatiotemporal variability of extreme summer precipitation over the Yangtze River basin and the associations with climate patterns. WaterSA 9 (11), 873.
Sun, G.N., Wang, M.H., 2008. Study on relation and distribution between vegetative coverage and land degradation in Inner Mongolia. J. Arid Land Resour. Environ. 22 (2), 140–144.
Sun, Y.L., Guo, P., Yan, X.D., 2010. Dynamics of vegetation cover and its relationship with climate change and human activities in Inner Mongolia. J. Nat. Resour. 25 (3), 407–414.
Suo, L.L., Huang, J.Y., Tan, B.K., 2008. The influence of winter arctic oscillation on maximum and minimum air temperature over China in winter. J. Trop. Meteorol. 24 (2), 163–168.
Swain, D.L., Horton, D.E., Deepti, S., Diffenbaugh, N.S., 2016. Trends in atmospheric patterns conducive to seasonal precipitation and temperature extremes in California. Sci. Adv. 2 (4), e1501344.
Varotsos, C.A., Ondov, J.M., Cracknell, A.P., Efstathiou, M.N., Assimakopoulos, M.Â., 2006. Long-range persistence in global aerosol index dynamics. Int. J. Remote Sens. 27 (16), 3593–3603.

Wan, S.Q., Gu, C.H., Kang, J.P., Zou, J.X., Hu, Y.L., Xu, S.S., 2010. Monthly extreme high-temperature response to atmospheric oscillation in China. Acta Phys. Sin. 59 (1), 676–682.
Wang, L., Zhen, L., Liu, X.L., Batkhishig, O., Wang, Q., 2008. Comparative studies on climate changes and influencing factors in central Mongolian Plateau region. Geogr. Res. 27 (1), 171–180.
Wang, L.X., Liu, H.M., Yang, J., 2010. Climatic change of Mu Us sandy land and its influence on vegetation coverage. J. Nat. Resour. 25 (12), 2030–2039.
Yan, H., Chen, W., Yang, F., Liu, J., Yunfeng, H.U., Yongzan, J.I., 2014. The spatial and temporal analysis of extreme climatic events in Inner Mongolia during the past 50 years. Geogr. Res. 33 (1), 13–22.
Yang, P., Xia, J., Zhang, Y., Hong, S., 2017. Temporal and spatial variations of precipitation in northwest China during 1960–2013. Atmos. Res. 183, 283–295.
You, L., Dai, X., Zhang, Y., 2010. Extreme precipitation events in Inner Mongolia in 1961–2008. Adv. Clim. Chang. Res. 6 (6), 411–416.
You, Q., Kang, S., Aguilar, E., Pepin, N., Flügel, W.A., Yan, Y., Xu, Y., Zhang, Y., Huang, J., 2011. Changes in daily climate extremes in China and its connection to the large scale atmospheric circulation during 1961–2003. Clim. Dyn. 36 (11—12), 2399–2417.
You, Q., Ren, G., Fraedrich, K., Kang, S., Ren, Y., Wang, P., 2013. Winter temperature extremes in China and their possible causes. Int. J. Climatol. 33 (6), 1444–1455.
Zanchettin, D., Rubino, A., Matei, D., Bothe, O., Jungclaus, J.H., 2013. Multidecadal-to-centennial SST variability in the MPI-ESM simulation ensemble for the last millennium. Clim. Dyn. 40 (5), 1–18.
Zhai, P.M., Pan, X.H., 2003. Change in extreme temperature and precipitation over northern China during the second half of the 20th century. Acta Geograph. Sin. 58, 1–10.
Zhang, X., Aguilar, E., Sensoy, S., Melkonyan, H., Tagiyeva, U., Ahmed, N., et al., 2005. Trends in Middle East climate extreme indices from 1950 to 2003. J. Geophys. Res. Atmos. 110 (D22), 3159–3172.
Zhang, Q., Singh, V.P., Li, J., Jiang, F., Bai, Y., 2012. Spatio-temporal variations of precipitation extremes in Xinxiang, China. J. Hydrol. Sci. 434–435 (2), 7–18.
Zhao, Y., He, C., Zhang, Q., 2012. Monitoring vegetation dynamics by coupling linear trend analysis with change vector analysis: a case study in the Xilingol steppe in northern China. Int. J. Remote Sens. 33 (1), 287–308.
Zhao, W., Wei, Z., Zheng, Z., Dong, W., 2016. Surface temperature and precipitation variation of pastoral transitional zone in northern China during 1964–2013. Plateau Meteorol. 35 (4), 979–988.
Zhou, L.T., Wu, R., 2010. Respective impacts of the East Asian winter monsoon and ENSO on winter rainfall in China. J. Geophys. Res.-Atmos. 115 (D2), 107. https://doi.org/10.1029/2009JD012502.